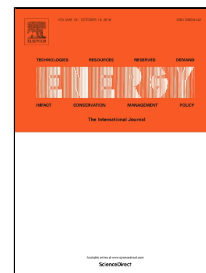


# Accepted Manuscript

Reverse Electrodialysis for energy production from natural River Water and Seawater

Ahmet H. Avci, Ramato A. Tufa, Enrica Fontananova, Gianluca Di Profio, Efrem Curcio



PII: S0360-5442(18)31875-9

DOI: 10.1016/j.energy.2018.09.111

Reference: EGY 13805

To appear in: *Energy*

Received Date: 26 February 2018

Accepted Date: 15 September 2018

Please cite this article as: Ahmet H. Avci, Ramato A. Tufa, Enrica Fontananova, Gianluca Di Profio, Efrem Curcio, Reverse Electrodialysis for energy production from natural River Water and Seawater, *Energy* (2018), doi: 10.1016/j.energy.2018.09.111

This is a PDF file of an unedited manuscript that has been accepted for publication. As a service to our customers we are providing this early version of the manuscript. The manuscript will undergo copyediting, typesetting, and review of the resulting proof before it is published in its final form. Please note that during the production process errors may be discovered which could affect the content, and all legal disclaimers that apply to the journal pertain.

# Reverse Electrodialysis for energy production from natural River Water and Seawater

Ahmet H. Avci<sup>1</sup>, Ramato A. Tufa<sup>2</sup>, Enrica Fontananova<sup>3</sup>, Gianluca Di Profio<sup>3</sup>, Efreem Curcio<sup>1,3\*</sup>

<sup>1</sup> Department of Environmental and Chemical Engineering, University of Calabria DIATIC-UNICAL, Via P. Bucci CUBO 45A, 87036 Rende (CS) Italy

<sup>2</sup> Department of Inorganic Technology, University of Chemistry and Technology Prague, Technická 5, 166 28 Prague 6, Czech Republic

<sup>3</sup> Institute on Membrane Technology, National Research Council of Italy ITM-CNR, Via P. Bucci CUBO 17C, 87036 Rende (CS) Italy

## Abstract

The effectiveness of Salinity Gradient Power - Reverse Electrodialysis (SGP-RE) in real practice is still not clearly defined due to the lack of specific studies in literature, being investigations in large part limited to pure NaCl solutions or aqueous mixtures of two salts. In this work, we experimentally assessed the impact of natural feed streams (collected from Licetto river and Tyrrhenian sea in Amantea - Italy) in terms of Open Circuit Voltage (OCV) and power density ( $P_d$ ) measured on a lab-scale SGP-RE stack prototype; results have been compared to those obtained when using NaCl solutions having equivalent ionic strength. Highest OCV (3.68 V and 4.09 V) and  $P_d$  values (0.46 and 1.41  $W \cdot m^{-2}$ ) were observed at temperature of 60°C for real and synthetic feeds, respectively.

The extent of electrical resistances (ion exchange membrane/electrical double layer/diffusion boundary layer) was elucidated by electrochemical impedance spectroscopy (EIS); in particular, a critical effect of real solution on cation exchange membrane (CEM) resistance was detected. Additionally, ionic characterization of process effluents revealed the occurrence of uphill transport of multivalent ions  $Mg^{2+}$ ,  $Ca^{2+}$  and  $SO_4^{2-}$ .

**Keywords:** *Reverse Electrodialysis; Salinity Gradient Power; natural feeds; Electrochemical Impedance Spectroscopy; Uphill transport*

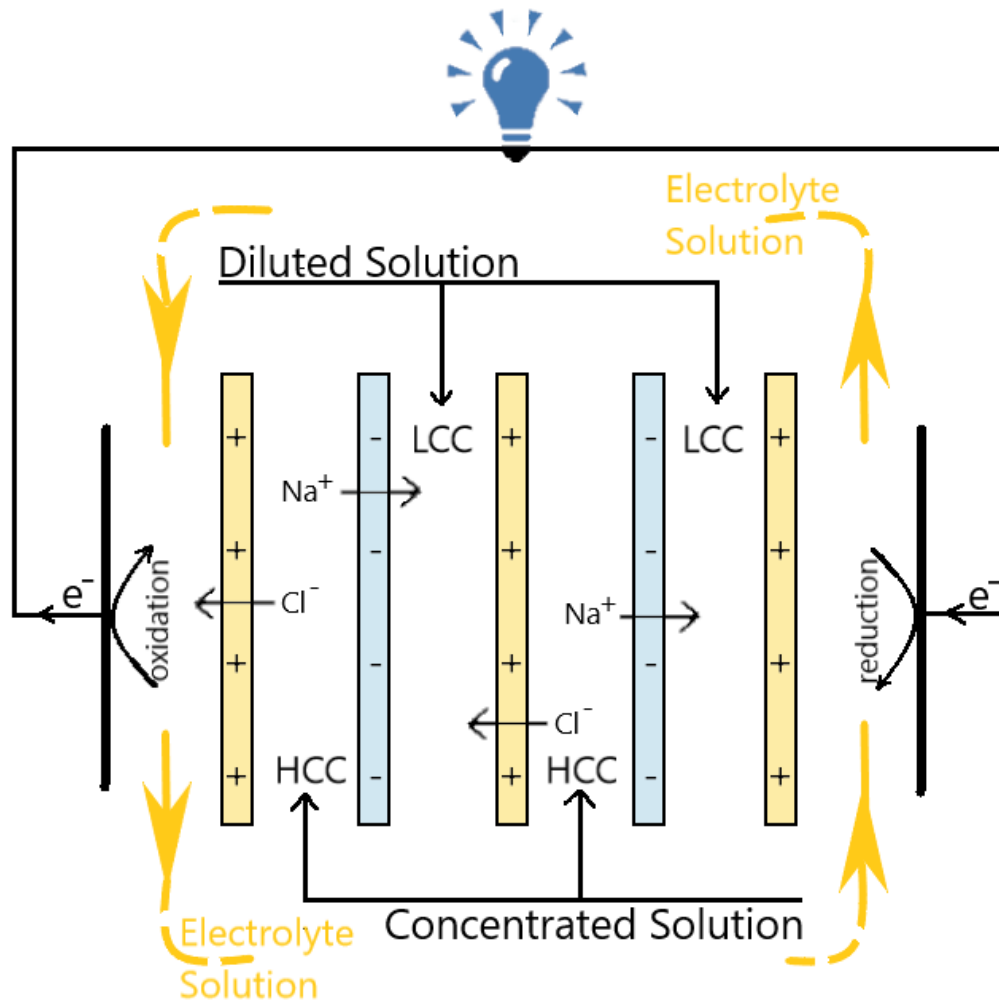
\* [e.curcio@unical.it](mailto:e.curcio@unical.it) (corresponding author)

## 1 **1. Introduction**

2 According to US Energy Information Administration, world net electricity generation is expected  
3 to increase from 20 trillion to 40 trillion kWh in the coming 30 years; among all sources which  
4 presently fulfill the increasing demand of energy, renewable energy is the fastest-growing source  
5 of electric power with an annual 2.8% increase [1]. An emerging renewable energy source is  
6 Salinity Gradient Power (SGP), originally proposed for sea and river water mixing more than 60  
7 years ago [2]. The total technical potential of SGP is estimated to be around 647 GW, which is  
8 23% of the global electricity consumption [3]. Possible application areas of SGP techniques are  
9 estuaries where freshwater rivers run into seawater [4–7], high salinity wastewater (brine from  
10 desalination [8–11] or salt mining and saltworks [12–14]) and saltwater lakes [15,16].

11 There are two common technologies which harvest SGP by utilizing membrane-based processes:  
12 Reverse Electrodialysis (SGP-RE) – object of the present work - and Pressure Retarded Osmosis  
13 (PRO) [17]. In a typical SGP-RE system, cation exchange membranes (CEM) and anion exchange  
14 membranes (AEM) are piled up alternately between cathode and anode (Fig. 1). CEMs and AEMs  
15 are separated by spacers to allow the diluted and concentrated salt solutions flowing through. Due  
16 to salinity gradient across the membranes, ions diffuse through the membranes from High  
17 Concentration Compartment (HCC) to Low Concentration Compartment (LCC): the ionic flux is  
18 converted to electronic flux in the electrode compartments by reduction and oxidation reactions  
19 on the electrode surface [10].

AC



1  
2 **Figure 1.** Conceptual scheme of a SGP-RE Unit

3  
4 The most abundant natural salinity gradient sources are seawater and river water. Theoretically,  
5 the generated mixing energy of two solution with different concentration can be calculated by  
6 Gibbs free energy equation [6]:

$$7 \quad \Delta G_{mix} = 2RT \left[ V_D C_D \ln \frac{C_D}{C_M} + V_C C_C \ln \frac{C_C}{C_M} \right] \quad (1)$$

$$1 \quad C_M = \frac{V_D C_D + V_C C_C}{V_D + V_C} \quad (2)$$

2 where  $\Delta G_{\text{mix}}$  is the Gibbs free energy of mixing,  $V_D$  is volume of diluted solution with  
3 concentration  $C_D$ ,  $V_C$  is volume of concentrated solution with concentration  $C_C$ ,  $C_M$  is the  
4 concentration of mixed solution,  $R$  is the gas constant ( $R=8.31432 \text{ Jmol}^{-1}\text{K}^{-1}$ ) and  $T$  is the  
5 temperature (K). Eq. 1 assumes enthalpy changes and activity of the solutions having negligible  
6 effect on final  $\Delta G_{\text{mix}}$ .

7 In theory, the complete mixing of  $1 \text{ m}^3$  seawater (assumed as  $30 \text{ kg} \cdot \text{m}^{-3}$  NaCl) and  $1 \text{ m}^3$  river water  
8 (assumed as pure water) produces  $1.7 \text{ MJ}$  energy, that can be increased up to  $6.1 \text{ MJ}$  at  $298 \text{ K}$  when  
9 volumetric ratio of river water/seawater is 10 [6]. The numerous attempts made to investigate  
10 extractable energy from seawater and river water mixing resulted in gross power density between  
11  $0.20 - 2.2 \text{ W} \cdot \text{m}^{-2}$  depending on membrane design [18–21], spacer design [7,22–24], stack design  
12 [25,26] and process conditions (i.e. concentration gradient, flow properties and temperature)  
13 [2,7,27,28]. One of the first measurements of power density was reported as  $0.20 \text{ W} \cdot \text{m}^{-2}$  by Pattle  
14 (1954). In that study, maximum power was obtained for polyethylene mixed with crosslinked  
15 polystyrene resins membranes and  $1 \text{ mm}$  nonconductive thickness at  $39^\circ\text{C}$  where  $0.5 \text{ M}$  NaCl  
16 solution and tap water were used as feed [2]. After IEM technology had improved, Veerman *et al.*  
17 performed synthetic seawater/river water SGP-RE experiments with six commercial membranes  
18 pairs; the highest measured power densities were  $1.17$  and  $1.18 \text{ W} \cdot \text{m}^{-2}$  for Fumasep (FAD and  
19 FDK) and Selemion (AMV and CMV) membrane pairs, respectively, and a noteworthy  
20 thermodynamic efficiency (35%) was obtained [18]. Guler *et al.* prepared custom-made sulfonated  
21 polyetheretherketone CEM and polyepichlorohydrin AEM designed for SGP-RE; utilizing these  
22 membrane pairs resulted in  $1.28 \text{ W} \cdot \text{m}^{-2}$  gross power density [20]. Hong *et al.* conducted  
23 experiments by pairing a custom-made composite CEM with ASV (Selemion, Japan) AEM; under

1 optimized electrochemical properties, a maximum power density of  $1.3 \text{ W}\cdot\text{m}^{-2}$  was generated [21].  
2 Vermaas *et al.* investigated the effect of intermembrane thickness and feed flow rate on the power  
3 density for synthetic seawater and river water: the highest recorded gross power density was  $2.2$   
4  $\text{W}\cdot\text{m}^{-2}$  for  $100 \mu\text{m}$  intermembrane thickness; moreover, possibility to reach  $4 \text{ W}\cdot\text{m}^{-2}$  was predicted  
5 for  $60 \mu\text{m}$  inter-membrane thickness [7].

6 Aforementioned studies, analogously with the large part of literature references, were carried out  
7 using synthetic solutions prepared only with NaCl or, seldom, with a mixture of inorganic salts to  
8 mimick natural feeds. However, a large spectra of mono- and multivalent ions together with some  
9 organic compounds are present in the natural feed solutions. Previous studies carried out on  
10 artificial multi-ion saline solutions revealed a drastic effect of these salts on the SGP-RE  
11 performance. Decrease in Nernst potential, uphill transport, increasing IEM resistance were the  
12 most pronounced observations due to presence of multivalent ions. Tufa *et al.* observed a 64%  
13 decrease in power density when a lab scale SGP-RE stack, installed with Fujifilm-80045 and  
14 Fujifilm-80050, was operated with artificial solutions  $0.083 \text{ M NaCl} + 0.017 \text{ M MgCl}_2/3.25 \text{ M}$   
15  $\text{NaCl} + 1.75 \text{ M MgCl}_2$  instead of  $0.1 \text{ M NaCl}/5 \text{ M NaCl}$  [10]. Avci *et al.* carried out a parametric  
16 work on concentration of  $\text{Mg}^{2+}$  for 0.5 and 4 molal solutions; having 100%  $\text{Mg}^{2+}$  instead of  $\text{Na}^+$   
17 resulted in more than 50% decrease on OCV, three times higher stack resistance and 90% decrease  
18 in produced gross power density [29]. Another study carried out with ground water (2.67 M) and  
19 seawater (0.79 M) showed that power generation was affected by the presence of divalent ions  
20 [30].

21 Vermaas *et al.* and Post *et al.* investigated the effect of divalent ions on stack voltage and resistance  
22 for artificial solutions mimicking seawater/river water pair: up to 50% reduction in power density  
23 was detected when  $\text{Mg}^{2+}$  and  $\text{SO}_4^{2-}$  ions were present [31,32].

1 Investigations on real environment are so far scarcely present in literature and those studies  
2 prevalently focus on fouling phenomena or on the overall stack performance. The first SGP-RE  
3 pilot plant was operated with natural brackish water and almost saturated brine from saltworks,  
4 and compared with artificial NaCl equivalent solutions by Tedesco *et al.*: the plant was able to  
5 generate 40 W power with 125 cell pairs and almost 50 m<sup>2</sup> membrane area for real waters whereas  
6 artificial NaCl solutions resulted in 65 W [14].

7 The key observation of Vermaas *et al.* for a stack operated with natural seawater and river water  
8 was a drastic decrease in power density (40 %) attributed to organic fouling and associated increase  
9 in pressure drop [33]. Pawlowski *et al.* investigated the performance of a SGP-RE stack fed with  
10 natural river water and seawater operated with relatively thick spacers (800 μm) [34,35]; the wider  
11 channels circumvented stack clogging and increase of pressure drop which was about 6 times  
12 lower than in Vermaas *et al.* [33]. However, none of these studies was supported by the  
13 electrochemical characterization of membranes exposed to natural feeds for a more comprehensive  
14 understanding of their impact on stack performance.

15 In the present study, the performance of SGP-RE was evaluated in a real environment by testing  
16 natural river water and seawater feeds. System performance was evaluated in terms of Open Circuit  
17 Voltage (OCV) and power density ( $P_d$ ) on a lab-scale SGP-RE stack prototype, and results  
18 compared to those obtained when using NaCl solutions with equivalent ionic strength. The extent  
19 of electrical resistances (ion exchange membrane/electrical double layer/diffusion boundary layer)  
20 was elucidated by electrochemical impedance spectroscopy (EIS). Occurrence of uphill transport  
21 due to the presence of multivalent ions ( $Mg^{2+}$ ,  $Ca^{2+}$  and  $SO_4^{2-}$ ) was investigated by ion  
22 chromatography.

## 1 2. Materials and Methods

### 2 2.1. Solutions

3 Natural feeds were collected from river Licetto and Tyrrhenian Sea in Amantea (Italy) and  
 4 processed through the SGP-RE stack without any treatment. In order to determine the ionic  
 5 composition, samples were collected, microfiltered through 0.20  $\mu\text{m}$  pore size polypropylene  
 6 membranes (Microdyn®) and analyzed by Ion Chromatography (see 2.3); data related to major  
 7 ions are reported in Table 1. Artificial aqueous solutions mimicking river water and seawater (same  
 8 ionic strength) were prepared by appropriate amounts of NaCl (Sigma Aldrich, Italy). Ionic  
 9 strength  $I_m$  of river and seawater was calculated as:

$$10 \quad I_m = \frac{1}{2} \sum m_i z_i^2 \quad (3)$$

11 where  $m_i$  is molality of the  $i$ -th ion and  $z_i$  its charge.

12 For SGP-RE operation, the composition of aqueous electrolyte solution was: 0.3 M potassium  
 13 hexacyanoferrate (II), 0.3 M potassium hexacyanoferrate (III) and 2.5 M sodium chloride (all  
 14 purchased from Sigma-Aldrich, Italy). For the preparation of synthetic saline solutions and  
 15 electrolyte solution, deionized water (PURELAB, Elga LabWaters,  $0.055 \text{ mS}\cdot\text{cm}^{-1}$ ) was used.

16

17 **Table 1.** Ionic composition of natural river water and seawater (major ions are reported) and  
 18 equivalent ionic strength.

	Concentration (ppm)									Ionic Strength (molal)
	Na <sup>+</sup>	K <sup>+</sup>	Mg <sup>2+</sup>	Ca <sup>2+</sup>	Cl <sup>-</sup>	NO <sub>2</sub> <sup>-</sup>	Br <sup>-</sup>	NO <sub>3</sub> <sup>-</sup>	SO <sub>4</sub> <sup>2-</sup>	
<b>River water</b>	23	4	28	152	16	0.5	-	2	78	0.012
<b>Seawater</b>	17941	671	2121	493	20975	-	117	63	2192	0.958

## 1 2.2. Reverse Electrodialysis setup

2 The SGP-RE lab-scale prototype provided by REDstack BV (The Netherlands) was used in the  
 3 same arrangement as described previously [29]. SGP-RE stack was equipped with AEM-80045  
 4 and CEM-80050 Ion Exchange Membranes (IEMs) provided by Fujifilm Manufacturing Europe  
 5 B.V. (The Netherlands). Relevant characteristics of the membranes are illustrated in Table 2.

7 **Table 2.** Properties of ion exchange membrane [36]

Membrane code	Thickness ( $\mu\text{m}$ )*	Ion exchange capacity (mmol/g membrane)	Density of fixed charge (mol/L)	Membrane areal resistance ( $\Omega\text{cm}^2$ )**
<b>Fuji-AEM-80045</b>	$129 \pm 2$	$1.4 \pm 0.1$	$3.8 \pm 0.2$	$1.551 \pm 0.001$
<b>Fuji-CEM-80050</b>	$114 \pm 2$	$1.1 \pm 0.1$	$2.4 \pm 0.2$	$2.974 \pm 0.001$

8 \*Conditions: NaCl 0.5 M, 20°C

9 \*\*Conditions: NaCl 0.5 M, 20°C, 2.8 cm/s

10  
 11 SGP-RE tests were carried out at different temperature (10-60 °C) and flow rate (20-40 L·h<sup>-1</sup>), as  
 12 detailed in Table 3. LCC and HCC solutions were fed to the stack at the same temperature and  
 13 flowrate; the flowrate of electrolyte solution was fixed to 30 L·h<sup>-1</sup>. Solutions were fed by  
 14 Masterflex L/S digital peristaltic pumps (Cole-Palmer, US) and conditioned to desired temperature  
 15 by a refrigerated/heated circulating bath (PolyScience, US) before entering into the stack.

16 A high dissipation five-decade resistance box in the range of 0.1–1000  $\Omega$  (CROPICO, Bracken  
 17 Hill, US) was used to load the SGP-RE system. Corresponding voltage drop and current were  
 18 recorded after altering resistance box in the range of 60–0.1  $\Omega$ . DC voltage drop across the stack  
 19 was measured by a 3½ digital multimeter with accuracy of 70.5% in the range of 200 mV to 200  
 20 V (Velleman, DVM760, Belgium), and the current flowing across the load resistors was measured  
 21 by 6½ digit multimeter (Agilent, 34422A, Italy).

1 Voltage (V) versus current (I) experimental data were fitted with a straight line mathematically  
 2 expressed by equation 4: here, the open circuit voltage ( $E_{OCV}$ ) and the total resistance of stack  
 3 ( $R_{stack}$ ) were respectively calculated as intercept ( $I=0$ ) and slope of the equation:

$$5 \quad V(I) = E_{OCV} - R_{stack} I \quad (4)$$

6 The gross power density  $P_d$  follows a parabolic trendline in the form of:

$$7 \quad P_d = \frac{E_{OCV}^2}{4R_{stack} N_M} \quad (5)$$

8 in which  $P_d$  is given in  $W \cdot m^{-2}$ ,  $E_{OCV}$  in V, and  $R_{stack}$  in  $\Omega \cdot m^2$ ;  $N_M$  is the number of membranes  
 9 contributing to the voltage.  $P_d$  reaches its maximum value when external resistance (load  
 10 resistance) is equal to internal resistance (stack resistance) [7].

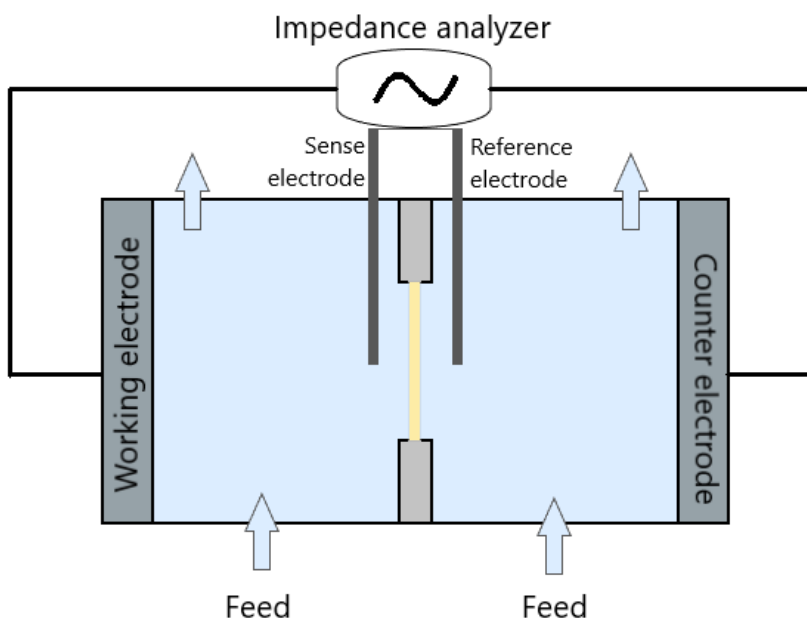
### 12 2.3. Ion Chromatography

13 Ion Chromatography was employed to quantify the concentration of ions at the inlet and outlet of  
 14 SGP-RE unit (Metrohm 861 Advanced Compact Ion Chromatography, Switzerland) operated  
 15 under experimental conditions detailed in Table 3, in open-circuit configuration (electrical load  
 16 disconnected) and continuous feed flow. In order to reach the steady-state, samples were collected  
 17 after one hour of operation. Samples were analyzed at room temperature, at which ion  
 18 chromatograph was calibrated. 3.2 mM  $Na_2CO_3$  + 1 mM  $NaHCO_3$  solution was used as eluent for  
 19 anion column Metrosep A Supp 5 - 250/4.0, and 2 mM nitric acid + 0.25 mM oxalic acid solution  
 20 was used as eluent for cation column Metrosep C4 - 250/4.0.

21

## 1 2.4. Electrochemical Impedance Spectroscopy

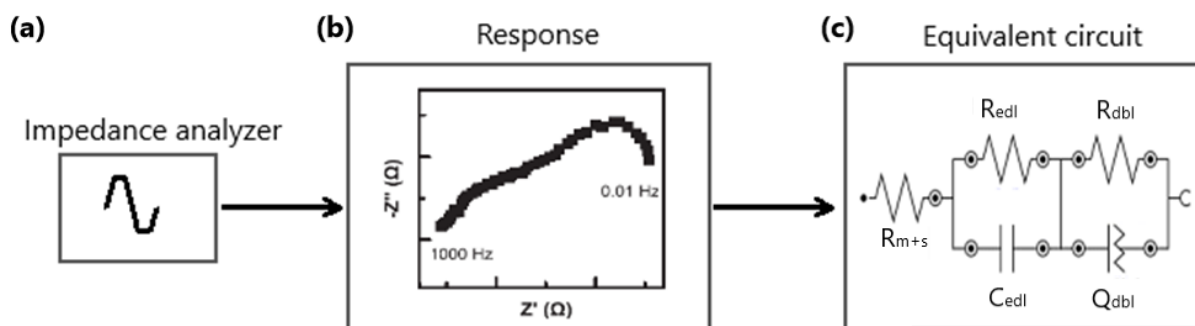
2 Electrochemical Impedance Spectroscopy (EIS) measurements were carried out using a  
 3 potentiostat/galvanostat combined with a frequency response analyzer (Metrohm Autolab  
 4 PGSTAT302N, Switzerland). A home-designed four electrodes impedance cell having 3.14 cm<sup>2</sup>  
 5 active membrane area (Fig. 2) was employed. Electro-deposition method was applied to cover  
 6 working and counter electrodes with a thin layer of AgCl. The sense and reference electrodes were  
 7 Ag/AgCl electrodes (Gamry Instruments); the Haber–Luggin capillaries were filled with 3 M KCl.



8  
 9 **Figure 2.** Scheme of four electrode configuration Electrochemical Impedance Spectroscopy (EIS)  
 10 cell. The same solution is fed on both compartments.

11  
 12 AEM-80045 and CEM-80050 membranes were characterized by EIS for natural sea and river  
 13 water at 25°C. Before analysis, virgin membranes were conditioned for 24 h in test solutions,  
 14 refreshed every 8 h to be sure no residual solutions were present.

1 Fig. 3 summarizes EIS procedure adopted in this study. AC current in the frequency range of 1000–  
 2 0.01 Hz with signal amplitude of 10 mV was generated through the cell and response was recorded.  
 3 Collected data were fitted by the equivalent circuit model shown in Fig. 3c by Nova 1.9.16 by  
 4 Metrohm Autolab B.V. (The Netherlands). Specifically, diffusion boundary layer was represented  
 5 by a resistor and a constant phase element in parallel, while electric double layer was represented  
 6 by a parallel combination of a resistor and a capacitor [36]. For each test solution, a blank  
 7 experiment (without membrane) was carried out in order to measure the solution resistance;  
 8 membrane resistance  $R_m$  is then calculated by subtracting solution resistance from overall  
 9 resistance ( $R_{m+s}$ ).



10  
 11 **Figure 3.** Summary of the EIS procedure: a) impedance analyzer; b) plot of real  $Z'$  (Ω) and  
 12 imaginary part  $Z''$  (Ω) of impedance; c) illustration of equivalent circuit for membrane and solution  
 13 resistance, electrical double layer resistance and diffusion boundary layer resistance.

## 15 2.5 Error analysis

16 All tests were repeated three times, and relevant experimental data averaged to estimate  
 17 measurements uncertainty.

18

### 1 3. Results and discussion

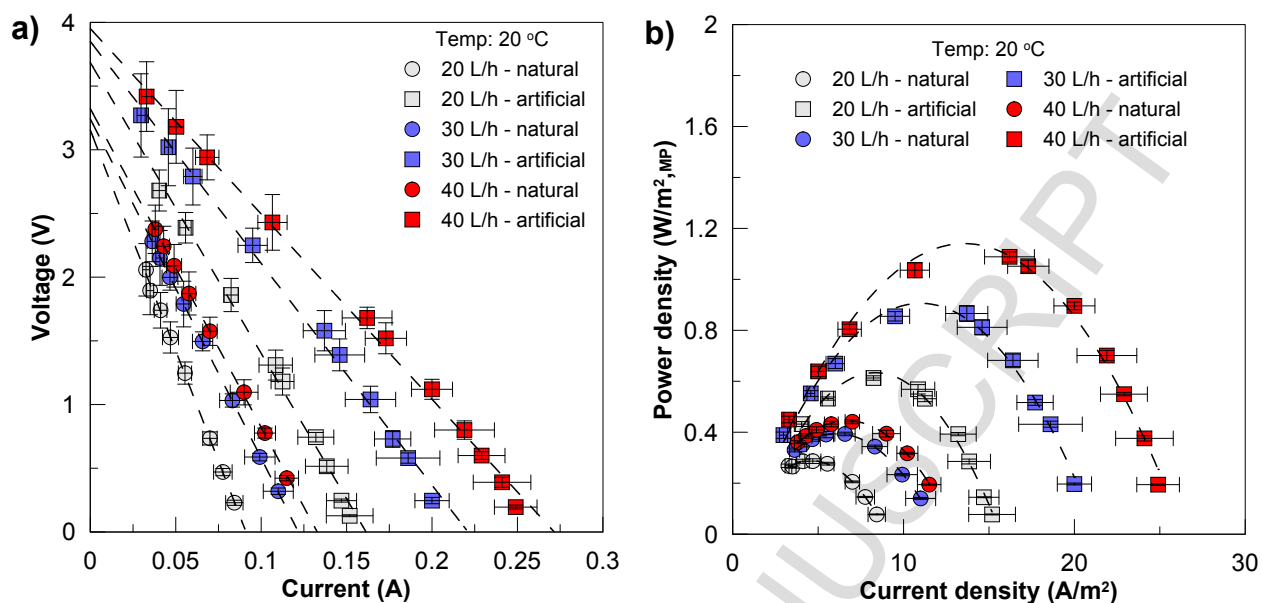
#### 2 3.1. SGP-RE tests

3 Natural seawater and river water under investigation contain 44.6 and 0.3 g/L of total dissolved  
4 salts, respectively. The ionic content is higher with respect to standard values reported in literature  
5 (35 g/L and 0.13 g/L, respectively); however, this salinity variation is an expected situation in  
6 restricted basins (i.e. Mediterranean sea) [37].

7 Fig. 4 illustrates current-voltage and current density-power density curves for natural and artificial  
8 solution at constant temperature of 20°C and at different flow rates. The maximum SGP-RE  
9 performance was observed for synthetic NaCl solutions fed at flow rate 40 L·h<sup>-1</sup>: gross P<sub>d</sub> reached  
10 a maximum of 1.14 W·m<sup>-2</sup> at current density of 15 A·m<sup>-2</sup>, OCV attained 3.96 V, and R<sub>stack</sub> was  
11 14.8 Ω. On the other hand, the poorest performance was detected when mixing natural seawater  
12 and river water at flow rate 20 L·h<sup>-1</sup>: gross P<sub>d</sub> value and current density fell down to 0.29 W·m<sup>-2</sup>  
13 and 5 A·m<sup>-2</sup>, respectively, while OCV decreased to 3.17 V and R<sub>stack</sub> increased to 34.9 Ω. Use of  
14 natural solutions instead of synthetic ones resulted in a reduction of power density higher than  
15 50%; this effect became more visible at higher flow rates. Eq. 5 illustrates the dependence of power  
16 density on OCV and R<sub>stack</sub>. Although OCV is more influential on power density (squared  
17 dependence), in our case the dominant decreasing parameter was R<sub>stack</sub>; in fact, OCV values varied  
18 within a quite narrow range (3.1 – 4.0 V), while R<sub>stack</sub> reduced significantly (from 35 to 14 Ω).

ACC

1



2

3 **Figure 4.** SGP-RE performance at 20°C and different flowrate: a) Voltage versus current; b) Gross  
4 power density versus current density.

5

6 Average permselectivity  $\alpha_{ave}$  of Fuji-AEM-80045 and Fuji-CEM-80050 membranes can be  
7 calculated from Planck Henderson equation [5]:

$$8 \quad E_{OCV} = 2N \frac{RT}{F} \frac{\alpha_{ave}}{z} \ln \left( \frac{a_s}{a_r} \right) \quad (6)$$

9 where N is number of membranes, R is the universal gas constant (J mol<sup>-1</sup>·K<sup>-1</sup>), T is the absolute  
10 temperature (K), F is the Faraday constant (C·mol<sup>-1</sup>),  $a_s$  is the activity of seawater solution  
11 (mol·l<sup>-1</sup>),  $a_r$  is the activity of river water solution (mol·l<sup>-1</sup>), and z is the ion valence (-). Activity  
12 coefficients were evaluated by PHREEQC v. 2.18.00 software [38].

13 Average permselectivity of the Fuji-AEM and CEM in artificial seawater and river water mixing  
14 was 68%, assuming a linear variation of solute concentration along the stack. As a comparison,  
15 Fontananova *et al.* reported permselectivity of Fuji-CEM and Fuji-AEM measured by *ex-situ*

1 method as 96% and 93% (average: 94.5%), respectively, in 0.1//0.5 M pure NaCl solutions [39].  
2 The lower permselectivity can be explained by the higher concentration gradient of feed solutions  
3 (from table 1, equivalent ionic strength is 0.012 and 0.958 molal for river water and seawater,  
4 respectively, for an HCC/LCC ratio of  $\sim 80$ ) that enhances the co-ion transport against the  
5 chemical potential gradient [39,40]. Accordingly, for 0.1//5.0 M NaCl solutions (HCC/LCC ratio  
6 of  $\sim 50$ ), Fontananova *et al.* observed a decrease of Fuji-CEM and Fuji-AEM permselectivity to  
7 89% and 73%, respectively [39].

8 Table 3 summarizes the experimental data for OCV, resistance and  $P_d$ . In general, a step increase  
9 in flowrate from 20 to 30 L·h<sup>-1</sup> improved  $P_d$  and decreased stack resistance more than a further  
10 increment from 30 to 40 L·h<sup>-1</sup>. For natural solutions, in the first case  $P_d$  enhanced by 38% while  
11  $R_{stack}$  decreased by 23% whereas, in the second step,  $P_d$  enhanced by 10% while  $R_{stack}$  decreased  
12 only by 7%. Likewise, when flowrate of artificial solution was increased from 20 L·h<sup>-1</sup> to 30  
13 L·h<sup>-1</sup>,  $P_d$  increased by 48% and  $R_{stack}$  decreased by 24%; these values were limited to 27% and 16%  
14 in the case of flowrate enhancement from 30 to 40 L·h<sup>-1</sup>. Vermaas *et al.* observed that the diffusive  
15 boundary layer near the membranes induces a considerable resistance at lower flow rates [7].  
16 Enhancing the non-ohmic resistances by improving fluid-dynamics (higher Reynolds number) is  
17 possible up to a certain extent; further increase in flow rate does not promote a significant gain in  
18 terms of gross  $P_d$  due to increase in pumping energy [41].

19 An additional reason for increasing power density at higher flow rates is related to the residence  
20 time of solutions within the stack. Higher residence time (at lower flowrate) results in a more  
21 significant dilution of the HCC solution accompanied by a more significant concentration of the  
22 LCC solution; the consequent decrease of concentration gradient across IEMs causes the decline  
23 of SGP-RE performance.

1 **Table 3.** Measured data from SGP-RE tests.

2

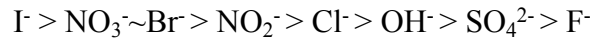
Flow rate L/h	Temp. °C	Natural Solutions			Artificial Solutions		
		OCV V	$R_{stack}$ $\Omega$	$P_d$ W/m <sup>2</sup>	OCV V	$R_{stack}$ $\Omega$	$P_d$ W/m <sup>2</sup>
20	60	3.68	30.5	0.46	4.09	12.8	1.41
	40	3.54	33.2	0.39	4.10	14.5	1.26
	20	3.17	34.9	0.29	3.69	23.1	0.61
	10	3.02	37.7	0.24	3.48	32.4	0.38
30	20	3.25	26.8	0.40	3.86	17.6	0.90
40	20	3.32	25.0	0.44	3.96	14.8	1.14

3

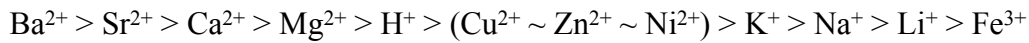
4 In natural seawater, more than 10%w of cations were divalent ions ( $Mg^{2+}$  and  $Ca^{+}$ ) and  
5 approximately 10%w of anions were divalent  $SO_4^{2-}$ . The evidence of the negative impact of  
6 divalent ions on the SGP-RE performance, is reported in literature [10,29,31,32,42]; hereafter we  
7 show that this effect - intrinsically associated to the ion valence  $z>1$  in equation 6 – is mainly  
8 enforced by the increase in IEM resistance and the occurrence of  $Mg^{2+}$  and  $SO_4^{2-}$  transport against  
9 its concentration gradient.

10 Membrane resistance and permselectivity are significantly affected by the electrical interactions  
11 between bi-valent ions and fixed charged groups of IEMs; in particular, an increase in CEM  
12 resistance occurs due to crosslinking of two fixed anionic groups when bridged by  $Mg^{2+}$ ; similarly,  
13  $SO_4^{2-}$  ions cause an increase of AEM resistance by attracting each one a pair of fixed cationic  
14 groups. Neutralization of some fixed groups reduces the effective charge density of IEMs;  
15 consequently, ineffective Donnan exclusion results in a low permselectivity [43]. Ion  
16 permselectivity depends on several factors, such as affinity of a specific ion to a given fixed group

1 on the membrane and mobility of ions. The selectivity order of anions were stated by Sata (2000)  
 2 [44] as:



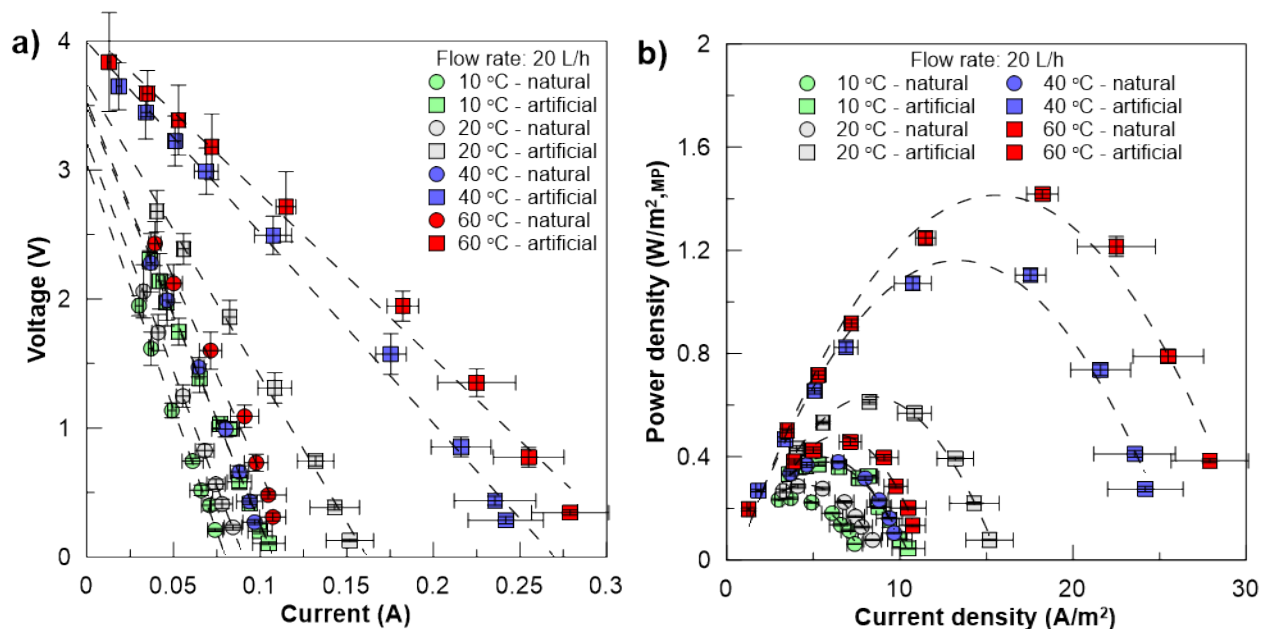
4 while selectivity order for cations were reported by Strathmann (2004) [45] as:



6 According to permselectivity studies, it can be concluded  $\text{Cl}^-$  is preferred against  $\text{SO}_4^{2-}$  by AEM  
 7 whereas  $\text{Ca}^{2+}$  and  $\text{Mg}^{2+}$  are preferred against  $\text{Na}^+$  by CEM. Coherently, Avci *et al.* observed that  
 8 CEM resistance is critically affected by  $\text{Mg}^{2+}$  concentration [29].

9 Fig. 5 shows the results from electrical tests on SGP-RE stack at different temperatures (10, 20,  
 10 40 and 60°C) for both natural and artificial seawater and river water. Under the same experimental  
 11 conditions, mixing artificial NaCl solutions resulted in higher  $P_d$  and OCV, and lower  $R_{\text{stack}}$  than  
 12 natural solutions. Presence of approximately 10%w multivalent ions reduced OCV due to the  
 13 screening effect of fixed charge groups on IEMs as discussed before. However, for both natural  
 14 and artificial solutions, the performance of SGP-RE unit increased with temperature due to higher  
 15 transport rate of ions. Diffusion coefficients of  $\text{Na}^+$  and  $\text{Cl}^-$  in 0.5 M NaCl were measured for Fuji-  
 16 CEM-80050 and Fuji-AEM-80045, respectively, at different temperatures by Fontananova *et al.*:  
 17 a 24% and 80% increase were recorded for chloride and sodium ions, respectively, when increasing  
 18 temperature from 20 to 40 °C [36]. At 60 °C, the maximum power density and OCV were 1.41  
 19  $\text{W}\cdot\text{m}^{-2}$  and 4.09 V, respectively, recorded for artificial feeds and  $R_{\text{stack}}$  reached its lowest value of  
 20 12.8  $\Omega$ . On the other hand, power density and OCV of natural feeds had a minimum at 0.24  
 21  $\text{W}\cdot\text{m}^{-2}$  and 3.02 V, respectively, when the experimental conditions were designed for winter  
 22 conditions at 10 °C.

23



1  
2  
3 **Figure 5.** SGP-RE performance at 20 L·h<sup>-1</sup> and different temperature: a) Voltage versus current;  
4 b) Gross power density versus current density.

5  
6 Besides SGP-RE performance under steady-state conditions, we investigated the dynamic  
7 behavior of the system with the aim to estimate how fast is its response to sudden changes in  
8 flowrate, assuming that temperature variations in fluvial and maritime basins take place on a broad  
9 time scale. Fig. 6 illustrates the OCV profile over time for flowrate step changes (increase by 10  
10 L/h every 20 minutes) at 20 °C. The response of the lab scale SGP-RE stack reveals that a new  
11 steady-state condition is reached after 0.75-1.50 minutes, i.e. 3-5 times the residence time of the  
12 feed solutions within the cells of the device.

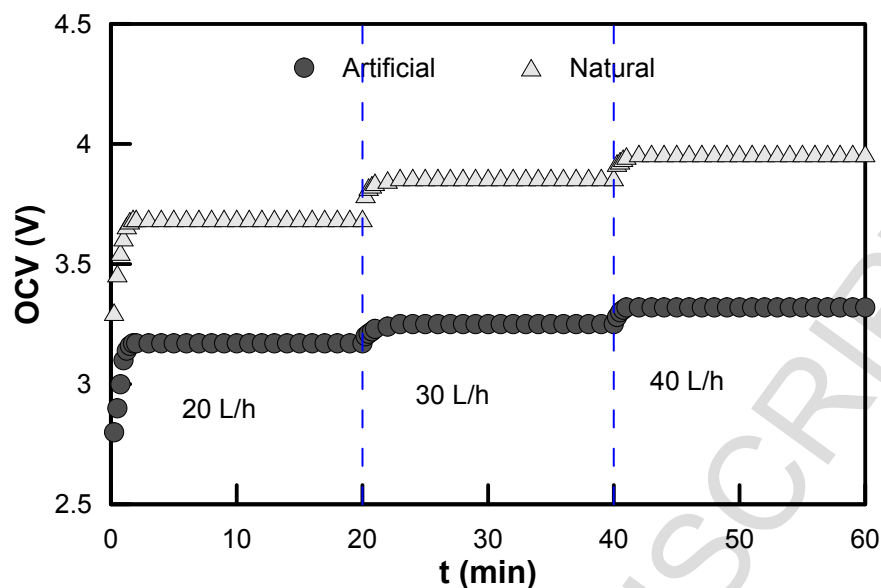


**Figure 6.** Dynamic response of OCV to step change in flowrate at 20 °C

### 3.2. Uphill transport

Characterization of ion concentration in the inlet and outlet streams is essential for a deep understanding of mixing process and transport phenomena taking place within the SGP-RE unit. This investigation is important from both chemical and physical point of view, since different ions exhibit a different level of interactions with fixed charge groups located on IEMs. Figure 7 illustrates the influence of flowrate on ion transport at constant temperature (20°C). As expected, increasing flowrate ended up with a decreased number of transported ions for major monovalent species ( $\text{Cl}^-$  and  $\text{Na}^+$ ) for both artificial and natural solutions due to lower residence time.  $\text{K}^+$ , a minor monovalent ion, also contributed to the total flux by transporting in the same direction of concentration gradient. On the other hand, multi-valent ions like  $\text{Mg}^{2+}$ ,  $\text{Ca}^{2+}$  and  $\text{SO}_4^{2-}$  showed transport along the opposite direction of concentration gradient; this phenomenon is known as “uphill transport” [29,31,32,42].

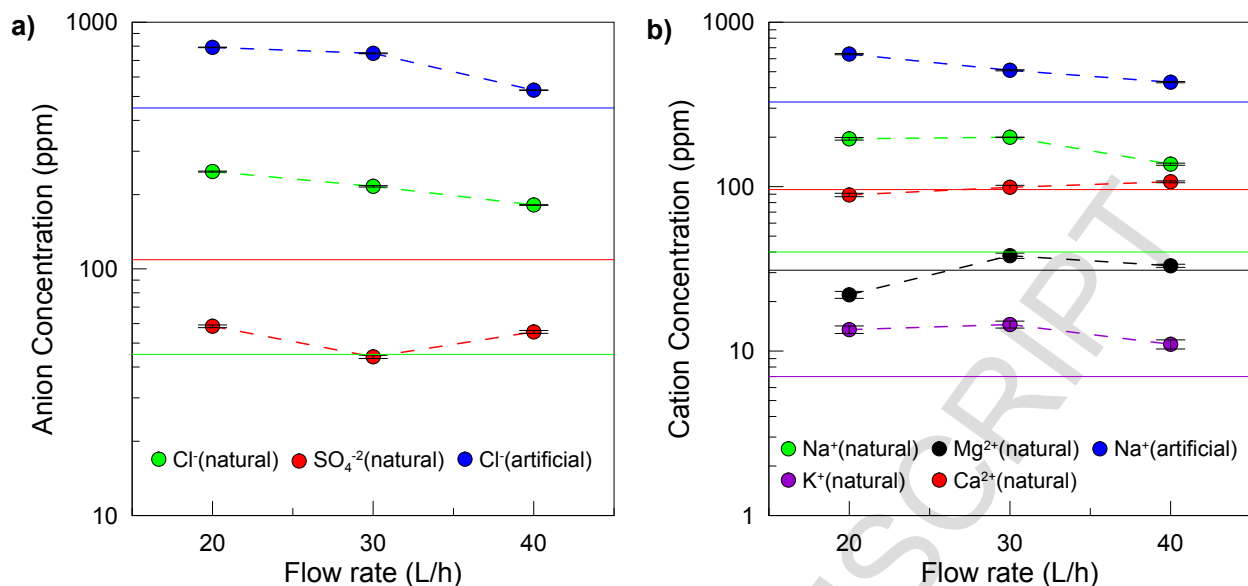
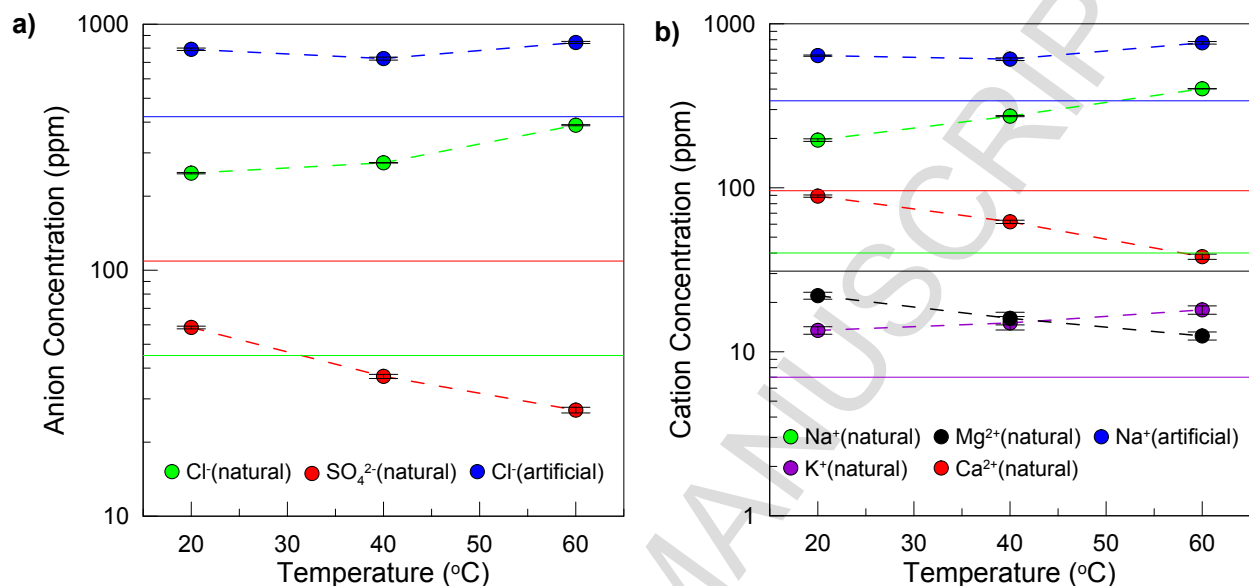


**Figure 7.** Transport of ions in LCC as a function of flowrate (temperature: 20°C): a) anions Cl<sup>-</sup>, SO<sub>4</sub><sup>2-</sup>; b) cations Na<sup>+</sup>, K<sup>+</sup>, Ca<sup>2+</sup> and Mg<sup>2+</sup>. Solid line with the same color of the symbol represents the inlet concentration of the corresponding ion, symbols are the outlet concentration of ions. Uphill transport occurs when symbols are below the corresponding solid lines.

Inter-diffusion between monovalent and multivalent ions occurs in other systems such as Donnan dialysis, driven by Donnan potential established between the membrane and the adjacent solution to maintain electroneutrality [31,32,42]. In SGP-RE, some previous studies carried out with artificial seawater and river water containing divalent ions, e.g. Mg<sup>2+</sup> and SO<sub>4</sub><sup>2-</sup>, reported the occurrence of uphill transport. Rijnaarts *et al.* theoretically explained the uphill transport over an ideal CEM exposed to 0.5 and 0.017 M saline solutions with 10% mol Mg<sup>2+</sup>; cations start moving across the ion selective membrane under Donnan potential (0.079 V for Na<sup>+</sup> and 0.039 V for Mg<sup>2+</sup>), until achieving Donnan equilibrium and maintaining charge neutrality (two Na<sup>+</sup> exchange for one Mg<sup>2+</sup>) [42]. Investigations of Avci *et al.* provided evidence of uphill transfer in SGP-RE operated with NaCl-MgCl<sub>2</sub> solutions in the range of 0-30% of Mg<sup>2+</sup> [29]. Fig. 8 shows the transported ions in LCC at temperatures of 20, 40 and 60°C with feed flowrate kept constant at 20 L·h<sup>-1</sup>. At increasing temperature, major monovalent ions exhibit a faster transport along the concentration

1 gradient, while multivalent ions  $\text{Ca}^{2+}$ ,  $\text{Mg}^{2+}$  and  $\text{SO}_4^{2-}$  resulted in uphill transport at increasing  
 2 mobility.

3



4

5 **Figure 8.** a) Transport of ions in LCC as a function of temperature (flowrate: 20 L·h<sup>-1</sup>): a) anions  
 6 Cl<sup>-</sup>, SO<sub>4</sub><sup>2-</sup>; b) cations Na<sup>+</sup>, K<sup>+</sup>, Ca<sup>2+</sup> and Mg<sup>2+</sup>. Solid line with the same color of the symbol  
 7 represents the inlet concentration of the corresponding ion, symbols are the outlet concentration of  
 8 ions. Uphill transport occurs when symbols are below the corresponding solid lines.

9

### 10 3.3. Electrochemical Impedance Spectroscopy

11 Characterization of electrical properties of IEMs and their interfaces was done by Electrochemical  
 12 Impedance Spectroscopy (EIS) [46]. In this study, a range of frequency from 0.01 to 1000 Hz was  
 13 applied to analyze impedance of the membranes and electrolytes. In such a system, the total  
 14 resistance is determined by ohmic resistances (i.e. membrane and solution resistances) and non-  
 15 ohmic resistances (i.e. electrical double layer and diffusion boundary layer resistances) as it is  
 16 shown by the electrical circuit (Fig. 3).

1 Charged groups fixed on the membrane surface attract the oppositely charged ions via Coulomb  
2 forces and create electrical double layer at the solid-liquid interface. Electrical double layer is  
3 composed of Stern layer and diffuse layer; strongly bounded ions - due to electrostatic interactions  
4 next to the membrane - form the Stern layer, while diffuse layer is caused by weak electrostatic  
5 interactions on the outer shell of electrical double layer [36].

6 Diffusion boundary layer arises from the difference between transport number of the membrane  
7 and the bulk solution. In an ideal IEM, electrical current is transported by counter ions because of  
8 the Donnan exclusion. On the other hand, in the bulk solution, univalent ions carry almost the same  
9 electrical current, and as a result, excluded ions get polarized as an additional layer [36].

10 EIS allowed the quantitative characterization of the different electrical resistances present in the  
11 system. In Fig. 9, the Nyquist plot of the frequency response for Fuji-AEM-80045 and Fuji-CEM-  
12 80050 exposed to natural seawater (Fig. 9.a) and river water (Fig. 9.b) shows the real (abscissa  
13 axis) and imaginary (ordinate axis) parts of the impedance. The extent of  $R_{m+s}$  is investigated at  
14 high frequency, i.e. 1000 Hz. Non-ohmic resistances,  $R_{edl}$  and  $R_{dbl}$ , were evaluated by fitting data  
15 with the equivalent circuit shown in Fig. 3.c. The Nyquist response of CEM shifted towards higher  
16 values compared to AEM, confirming a significantly greater ohmic resistance of the cation  
17 exchange membrane. Similarly, enlarged amplitude of the Nyquist curves when moving from  
18 seawater to river water qualitatively indicates an increase in the non-ohmic resistance.

19

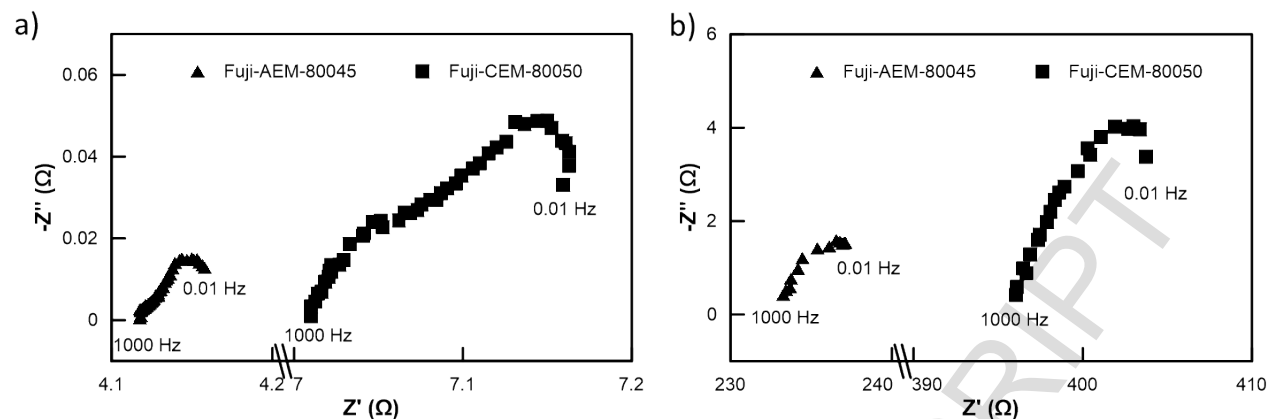
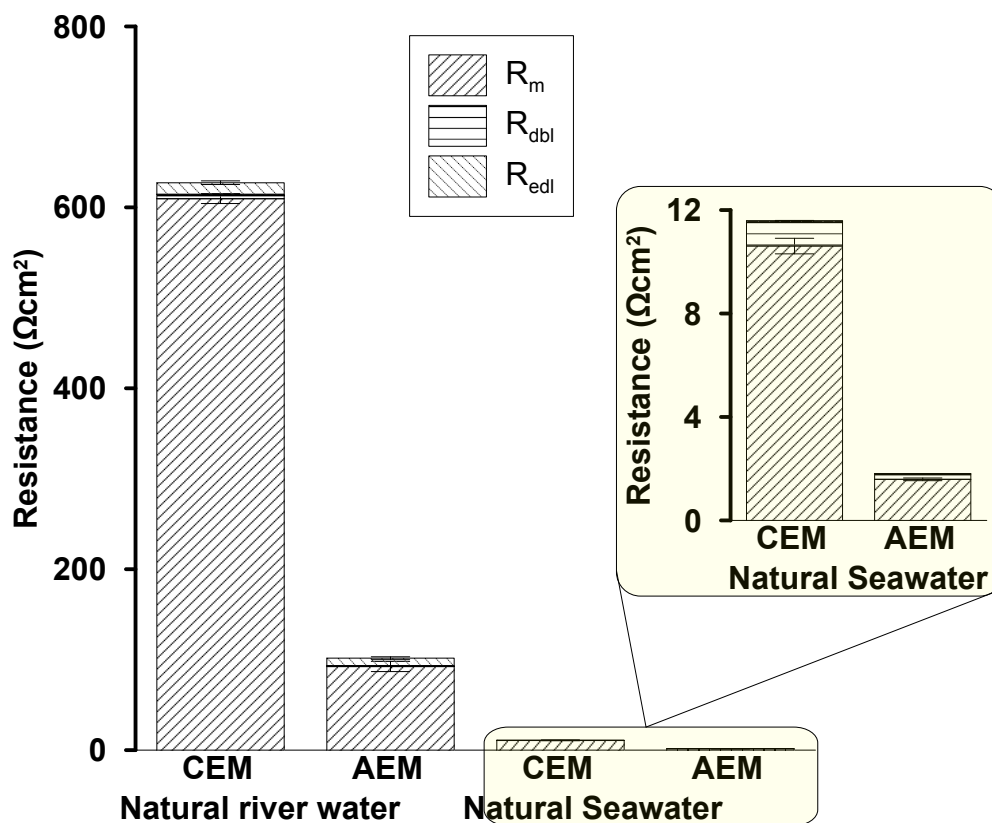


**Figure 9.** Nyquist plot of the Fuji-AEM-80045 and Fuji-CEM-80050 at 20 °C in: a) natural seawater and b) natural river water.

Fig. 10 illustrates the extent of ohmic and non-ohmic resistances when AEM-80045 and CEM-80050 membranes are operated in natural feed streams. As expected, total membrane resistances were an order of magnitude higher when natural river water used. In particular, CEM offers 5-6 times higher resistance than AEM in both seawater and river water, confirming the high impact of divalent cations. The aforementioned charge screening effect by divalent ions cause neutralization of fixed charge groups and, ultimately, increase of membrane resistance. It is worth mentioning that, for all cases, the extent of non-ohmic resistances was negligible with respect to total resistance.

The increase in the stack resistance when feed streams were shifted from artificial to natural solutions can be therefore attributed prevalently to the increase in CEM resistance. When comparing the values of membrane resistance with respect to measurements in standard solutions presented in Table 2, no significant change was observed for AEM, while CEM resistance increased 5 times in natural seawater. A possible explanation is that the affinity of fixed charged groups of a CEM to  $\text{Na}^+$  is lower than that of multivalent ions such as  $\text{Mg}^{2+}$  and  $\text{Ca}^{2+}$  whereas, for AEM, the affinity to  $\text{Cl}^-$  is higher than that of  $\text{SO}_4^{2-}$ , thus determining a limited screening effect.

1



2

3 **Figure 10.** Ohmic and non-ohmic resistances for AEM-80045 and CEM-80050 operated in natural  
 4 river water and seawater ( $R_m$ : membrane resistance;  $R_{dbl}$ : diffusive boundary layer resistance;  $R_{edl}$ :  
 5 electrical double layer resistance).

6

7 The high resistance of IEMs in natural river water is coherent with the studies of Galama *et al.*,  
 8 who noted that membrane resistance mostly depends on the lowest external solution ion  
 9 concentration and, below 0.3 M, it is limited by the conductivity of ionic solution [47].

10 Concerning the non-ohmic resistances, electrical double layer and diffusion boundary layer  
 11 resistances were, respectively, one and two order of magnitude lower than ohmic resistances, for  
 12 both AEM and CEM. Non-ohmic resistances in river water were about 10 times lower than those  
 13 measured in seawater. For natural seawater, non-ohmic resistances on CEM were higher than on

1 AEM because of the higher different mobility of chloride with respect to sodium ( $u_{\text{Cl}^-}/u_{\text{Na}^+} = 1.5$   
2 [48]). Dlugulecki *et al.* observed that non-ohmic resistances are affected by the hydrodynamics of  
3 the system; on the other hand, ohmic resistances depend on temperature [48]. The values of total  
4 stack resistance reported in Table 3 agree with these assumptions: increasing flowrate from 20 to  
5 40 L·h<sup>-1</sup> resulted in 42% and 36% reduction in  $R_{\text{stack}}$  for natural and artificial solutions,  
6 respectively. Moreover, raising the temperature from 20 °C to 60 °C led to 13% and 44% reduction  
7 of  $R_{\text{stack}}$  for natural and artificial solutions, respectively.

8

#### 9 **4. Conclusion**

10 Tests with natural feeds provide reliable data on the realistic potential and current technical  
11 limitation of SGP-RE. In this study, energy generation by mixing natural seawater/river water and  
12 equivalent (in terms of ionic strength) NaCl solutions was investigated at different temperatures  
13 and flow rates. All artificial solutions resulted in higher power density, higher OCV and lower  
14  $R_{\text{stack}}$ . At best, 1.41 W·m<sup>-2</sup> maximum gross power density was extracted when operating with  
15 artificial NaCl solutions at 60 °C, showing highest OCV (3.68 V) and lowest  $R_{\text{stack}}$  (30.5 Ω). On  
16 the other hand, SGP-RE performance with natural feeds was significantly reduced as a result of  
17 increased membrane resistance, reduced OCV and occurrence of uphill transport for Ca<sup>2+</sup>, Mg<sup>2+</sup>  
18 and SO<sub>4</sub><sup>2-</sup>. Electrochemical impedance spectroscopy demonstrated that the decrease of system  
19 performance was prevalently due to the significant increase of CEM resistance. The areal  
20 resistance for CEM in natural seawater reached up to 10.6 Ωcm<sup>2</sup> which is about 3.5 times that of  
21 the areal resistance detected for artificial solutions (3.0 Ωcm<sup>2</sup>). These results mark a substantial  
22 difference from the membrane resistance traditionally measured in 0.5 M NaCl solutions which,  
23 typically, varies in the range of 0.9 – 3.1 Ωcm<sup>2</sup> for homogeneous CEMs [49]. The observed trend

1 of membrane resistance under realistic natural feeds reported in the present study elucidates the  
2 behavior of IEMs as a premise for an optimal design of materials and of manufacturing strategies  
3 necessary to enhance both the transport efficiency of monovalent ions and the rejection of  
4 multivalent ions [50].

5 In addition, results revealed the necessity to implement appropriate pretreatment to soften feed  
6 solutions, and to evaluate the impact of techno-economic requirements on practical application of  
7 SGP-RE.

## 8 **Acknowledgments**

9 The financial support of the Education, Audiovisual and Culture Executive Agency (EACEA-EU)  
10 within the programme EUDIME “Erasmus Mundus Doctorate in Membrane Engineering” (FPA  
11 2011–0014, SGA 2014–0970, <http://eudime.unical.it>) is kindly acknowledged.

## 13 **References**

- 14 [1] International Energy Outlook 2013,  
15 [https://www.eia.gov/outlooks/ieo/pdf/0484\(2013\).pdf](https://www.eia.gov/outlooks/ieo/pdf/0484(2013).pdf); 2013 (accessed in 22 February  
16 2018)
- 17 [2] Pattle RE, Production of electric power by mixing fresh and salt water in the hydroelectric  
18 pile, *Nature* 1954; 174:660.
- 19 [3] Ruud Kempener FN, Salinity gradient energy,  
20 [http://eusew.eu/sites/default/files/energy\\_days/Sal%20Grad%20Background%20doc%20.](http://eusew.eu/sites/default/files/energy_days/Sal%20Grad%20Background%20doc%20.pdf)  
21 [pdf](http://eusew.eu/sites/default/files/energy_days/Sal%20Grad%20Background%20doc%20.pdf). 2014 (accessed in 22 February 2018)
- 22 [4] Daniilidis A, Vermaas DA, Herber R, Nijmeijer K, Experimentally obtainable energy from  
23 mixing river water, seawater or brines with reverse electrodialysis, *Renew. Energy*. 2014;  
24 64:123–31.
- 25 [5] Weinstein JN, Leitz FB, Electric Power from Differences in Salinity: The Dialytic Battery,  
26 *Science* 1976; 191:557–9.

- 1 [6] Veerman J, Saakes M, Metz SJ, Harmsen GJ, Reverse electrodialysis: Performance of a  
2 stack with 50 cells on the mixing of sea and river water, *J. Memb. Sci.* 2009; 327:136–44.
- 3 [7] Vermaas DA, Saakes M, Nijmeijer K, Doubled power density from salinity gradients at  
4 reduced intermembrane distance, *Environ. Sci. Technol.* 2011; 45:7089–95.
- 5 [8] Brauns E, An alternative hybrid concept combining seawater desalination, solar energy and  
6 reverse electrodialysis for a sustainable production of sweet water and electrical energy,  
7 *Desalin. Water Treat.* 2010; 13:53–62.
- 8 [9] Tufa RA, Rugiero E, Chanda D, Hnàt J, van Baak W, Veerman J, Fontananova E, Di Profio  
9 G, Drioli E, Bouzek K, Curcio E, Salinity gradient power-reverse electrodialysis and  
10 alkaline polymer electrolyte water electrolysis for hydrogen production, *J. Memb. Sci.*  
11 2016; 514:155–64.
- 12 [10] Tufa RA, Curcio E, Van Baak W, Veerman J, Grasman S, Fontananova E, Di Profio G,  
13 Potential of brackish water and brine for energy generation by salinity gradient power-  
14 reverse electrodialysis (SGP-RE), *RSC Adv.* 2014; 4:42617–23.
- 15 [11] Tufa RA, Curcio E, Brauns E, Van Baak W, Fontananova E, Di Profio G, Membrane  
16 Distillation and Reverse Electrodialysis for Near-Zero Liquid Discharge and low energy  
17 seawater desalination, *J. Memb. Sci.* 2015; 496:325–33.
- 18 [12] Turek M, Bandura B, Dydo P, Power production from coal-mine brine utilizing reversed  
19 electrodialysis, *Desalination.* 1008; 221:462–6.
- 20 [13] Tedesco M, Brauns E, Cipollina A, Micale G, Modica P, Russo G, Helsen J, Reverse  
21 Electrodialysis with saline waters and concentrated brines: a laboratory investigation  
22 towards technology scale-up, *J. Memb. Sci.* 2015; 492:9–20.
- 23 [14] Tedesco M, Scalici C, Vaccari D, Cipollina A, Tamburini A, Micale G, Performance of the  
24 first Reverse Electrodialysis pilot plant for power production from saline waters and  
25 concentrated brines, *J. Memb. Sci.* 2016; 500:33–45.
- 26 [15] Emdadi A, Gikas P, Farazaki M, Emami Y, Salinity gradient energy potential at the hyper  
27 saline Urmia Lake - Zarrineh Rud River system in Iran, *Renew. Energy.* 2016; 86:154–62.
- 28 [16] Wick GL, Power from salinity gradients, *Energy.* 1978; 3:95–100.
- 29 [17] Post JW, Veerman J, Hamelers HVM, Euverink GJW, Metz SJ, Nymeiijer K, Buisman  
30 CJN, Salinity-gradient power: Evaluation of pressure-retarded osmosis and reverse  
31 electrodialysis, *J. Memb. Sci.* 2007; 288:218–30.

- 1 [18] Veerman J, de Jong RM, Saakes M, Metz SJ, Harmsen GJ, Reverse electro dialysis:  
2 Comparison of six commercial membrane pairs on the thermodynamic efficiency and  
3 power density, *J. Memb. Sci.* 2009; 343:7–15.
- 4 [19] Güler E, Elizen R, Saakes M, Nijmeijer K, Micro-structured membranes for electricity  
5 generation by reverse electro dialysis, *J. Memb. Sci.* 2014; 458:136–48.
- 6 [20] Güler E, Elizen R, Vermaas DA, Saakes M, Nijmeijer K, Performance-determining  
7 membrane properties in reverse electro dialysis, *J. Memb. Sci.* 2013; 446:266–76.
- 8 [21] Hong JG, Chen Y, Nanocomposite reverse electro dialysis (RED) ion-exchange membranes  
9 for salinity gradient power generation, *J. Memb. Sci.* 2014; 460:139–47.
- 10 [22] Veerman J, Post JW, Saakes M, Metz SJ, Harmsen GJ, Reducing power losses caused by  
11 ionic shortcut currents in reverse electro dialysis stacks by a validated model, *J. Memb. Sci.*  
12 20089; 310:418–30.
- 13 [23] Vermaas DA, Saakes M, Nijmeijer K, Enhanced mixing in the diffusive boundary layer for  
14 energy generation in reverse electro dialysis, *J. Memb. Sci.* 2014; 453:312–9.
- 15 [24] Długołęcki P, Dąbrowska J, Nijmeijer K, Wessling M, Ion conductive spacers for increased  
16 power generation in reverse electro dialysis, *J. Memb. Sci.* 2010; 347:101–7.
- 17 [25] Veerman J, Saakes M, Metz SJ, Harmsen GJ, Electrical power from sea and river water by  
18 reverse electro dialysis: a first step from the laboratory to a real power plant, *Environ. Sci.*  
19 *Technol.* 2010; 44:9207–12.
- 20 [26] Jagur-Grodzinski J, Kramer R, Novel process for direct conversion of free energy of  
21 mixing into electric power, *Ind. Eng. Chem. Process Des. Dev.* 1986; 25:443–9.
- 22 [27] Suda F, Matsuo T, Ushioda D, Transient changes in the power output from the  
23 concentration difference cell (dialytic battery) between seawater and river water, *Energy.*  
24 2007; 32:165–73.
- 25 [28] Turek M, Bandura B, Renewable energy by reverse electro dialysis, *Desalination.* 2007;  
26 205:67–74.
- 27 [29] Avci AH, Sarkar P, Tufa RA, Messana D, Argurio P, Fontananova E, Di Profio G, Curcio  
28 E, Effect of Mg<sup>2+</sup> ions on energy generation by Reverse Electro dialysis, *J. Memb. Sci.*  
29 2016; 520:499–506.
- 30 [30] Farrell E, Hassan MI, Tufa RA, Tuomiranta A, Avci AH, Politano A, Curcio E, Arafat  
31 HA, Reverse electro dialysis powered greenhouse concept for water- and energy-self-  
32 sufficient agriculture, *Appl. Energy.* 2017; 187:390–409.

- 1 [31] Vermaas DA, Veerman J, Saakes M, Nijmeijer K, Influence of multivalent ions on  
2 renewable energy generation in reverse electrodialysis, *Energy Environ. Sci.* 2014;  
3 7:1434–45.
- 4 [32] Post JW, Hamelers HVM, Buisman CJN, Influence of multivalent ions on power  
5 production from mixing salt and fresh water with a reverse electrodialysis system, *J.*  
6 *Memb. Sci.* 2009; 330: 65–72.
- 7 [33] Vermaas DA, Kunteng D, Saakes M, Nijmeijer K, Fouling in reverse electrodialysis under  
8 natural conditions., *Water Res.* 2013; 47:1289–98.
- 9 [34] Pawlowski S, Galinha CF, Crespo JG, Velizarov S, Prediction of reverse electrodialysis  
10 performance by inclusion of 2D fluorescence spectroscopy data into multivariate statistical  
11 models, *Sep. Purif. Technol.* 2015; 150:159–69.
- 12 [35] Pawlowski S, Galinha CF, Crespo JG, Velizarov S, 2D fluorescence spectroscopy for  
13 monitoring ion-exchange membrane based technologies - Reverse electrodialysis (RED),  
14 *Water Res.* 2016; 88:184–98.
- 15 [36] Fontananova E, Zhang W, Nicotera I, Simari C, van Baak W, Di Profio G, Curcio E, Drioli  
16 E, Probing membrane and interface properties in concentrated electrolyte solutions, *J.*  
17 *Memb. Sci.* 2014; 459:177–89.
- 18 [37] Kennish MJ, *Practical Handbook of Marine Science*, 3th ed., Boca Raton, FL: CRC Press  
19 LLC; 2001.
- 20 [38] Parkhurst DL, Appelo CAJ, *User's Guide To PHREEQC (version 2) — a Computer*  
21 *Program for Speciation Batch-Reaction, One-Dimensional Transport, and Inverse*  
22 *Geochemical Calculations*, *Water-Resources Investig. Rep.* 1999: 99-4259
- 23 [39] Fontananova E, Messana D, Tufa RA, Nicotera I, Kosma V, Curcio E, Van Baak W, Drioli  
24 E, Di Profio G, Effect of solution concentration and composition on the electrochemical  
25 properties of ion exchange membranes for energy conversion, *J. Power Sources.* 2017;  
26 340:282–93.
- 27 [40] Zlotorowicz A, Strand RV, Burheim OS, Kjelstrup S, The permselectivity and water  
28 transference number of ion exchange membranes in reverse electrodialysis, *J. Memb. Sci.*  
29 2017; 523:402–8.
- 30 [41] Pawlowski S, Rijnaarts T, Saakes M, Nijmeijer K, Crespo JG, Improved fluid mixing and  
31 power density in reverse electrodialysis stacks with chevron-profiled membranes, *J.*  
32 *Memb. Sci.* 2017; 531:111–21.

- 1 [42] Rijnaarts T, Huerta E, Van Baak W, Nijmeijer K, Effect of Divalent Cations on RED  
2 Performance and Cation Exchange Membrane Selection to Enhance Power Densities,  
3 Environ. Sci. Technol. 2017; 51:13028–35.
- 4 [43] Geise GM, Paul DR, Freeman BD, Fundamental water and salt transport properties of  
5 polymeric materials, Prog. Polym. Sci. 2014; 39:1–42.
- 6 [44] Sata T, Studies on anion exchange membranes having permselectivity for specific anions  
7 in electrodialysis - effect of hydrophilicity of anion exchange membranes on  
8 permselectivity of anions, J. Memb. Sci. 2000; 167:1–31.
- 9 [45] Strathmann H, Ion-Exchange Membrane Separation Processes, Amsterdam, The  
10 Netherlands, Elsevier B.V, 2004.
- 11 [46] Barsoukov E, Macdonald JR, Impedance Spectroscopy Theory, Experiment, and  
12 Applications, 2nd ed. Hoboken, New Jersey, Wiley-Interscience, 2005.
- 13 [47] Galama AH, Vermaas DA, Veerman J, Saakes M, Rijnaarts HHM, Post JW, Nijmeijer K,  
14 Membrane resistance: The effect of salinity gradients over a cation exchange membrane,  
15 J. Memb. Sci. 2014; 467:279–91.
- 16 [48] Długolecki P, Ogonowski P, Metz SJ, Saakes M, Nijmeijer K, Wessling M, On the  
17 resistances of membrane, diffusion boundary layer and double layer in ion exchange  
18 membrane transport, J. Memb. Sci. 2010; 349:369–79.
- 19 [49] Hong JG, Zhang B, Glabman S, Uzal U, Dou X, Zhang H, Wei X, Chen Y, Potential ion  
20 exchange membranes and system performance in reverse electrodialysis for power  
21 generation: A review, J. Memb. Sci. 2015; 486:71–88.
- 22 [50] Tufa RA, Pawlowski S, Veerman J, Bouzek K, Fontananova E, Di Profio G, Velizarov S,  
23 Crespo JG, Nijmeijer K, Curcio E, Progress and prospects in reverse electrodialysis for  
24 salinity gradient energy conversion and storage, Appl. Energy 2018; 225: 290-331.

**Highlights**

- Loss of power density is observed for SGP-RE operated with natural feeds.
- Electrochemical Impedance Spectroscopy shows a major impact on CEM resistance.
- A negligible impact of non-ohmic resistances is observed.
- Uphill transport of multivalent ions  $Mg^{2+}$ ,  $Ca^{2+}$  and  $SO_4^{2-}$  is detected.